Hindawi
Science and Technology of Nuclear Installations
Volume 2019, Article ID 1272156, 10 pages
https://doi.org/10.1155/2019/1272156

Research Article

Boiling Heat Transfer and Critical Heat Flux Enhancement Using Electrophoretic Deposition of SiO_2 Nanofluid

Aref Rahimian, Hosein Kazeminejad, Hosein Khalafi, Azam Akhavan, and Seyed Mohammad Mirvakili

Nuclear Science and Technology Research Institute (NSTRI), P.O. Box 11365-3486, Tehran, Iran

Correspondence should be addressed to Aref Rahimian; arahimian@aeoi.org.ir

Received 4 June 2019; Revised 17 August 2019; Accepted 15 November 2019; Published 28 December 2019

Academic Editor: Iztok Tiselj

The electrophoretic deposition (EPD) technique was used to create a uniform SiO_2 thin film coating on boiling plates, 4 mm in width and 9 mm in length. Significant enhancement in critical heat flux (CHF), for the hydrophilic surfaces generated by this anodic EPD method, has been observed. In order to increase the coating strength, the plates were sintered at various temperatures. To find the thickness and uniformity of the coatings, the SEM images were captured. The captured images showed that the coating thickness uniformly increased up to 90 nm for 0.5% nanofluid percentage by the EPD method. The results show that the hydrophilic and super-hydrophilic surfaces have different boiling heat transfer (BHT) coefficients and CHF behaviors. Also, the results showed an increase of 160% in the CHF value by sintering compared to a bare surface. However, because of the setup simplicity, the shape independency, the particle-coating uniformity, and thickness controllability, the EPD technique can be an appropriate option for modification of the surface and coating on the nuclear fuel cladding.

1. Introduction

One of the efficient heat transfer mood in the nuclear power plants is the nucleate boiling. In this heat transfer regime, the high heat flux can be transferred with smaller wall superheat than other heat transfer regimes. The nucleate boiling regime in the heat transfer systems is limited by the onset of nucleate boiling (ONB) and critical heat flux (CHF). The CHF phenomenon is a transition from the nucleate boiling with a high heat transfer to the film boiling by which heat is removed from the surface by vapor, whereby the heat transfer coefficient is rapidly decreased and the surface temperature is sharply increased with system failure. Therefore, the physical phenomenon of the CHF and its enhancement is an important part in the development of the nuclear thermal hydraulics.

Recent studies of boiling heat transfer have shown that the nanofluids can significantly improve the CHF. These nanofluids are the nanoparticles such as metal oxides, allotropes of carbon, or metals dispersed in base fluids [1]. CHF and boiling heat transfer coefficient have been investigated in the nanofluids boiling heat transfer studies [2–4], whereby these phenomena have changed with the dilute nanofluids. Further studies have shown that these changes in the nanofluid boiling phenomenon and CHF are not due to the intrinsic nature of the nanofluids but are due to the deposition of the nanoparticles on the heating surfaces and change of surface texture and morphology [5–8].

Enhancement of the CHF and boiling heat transfer by surface modification is not a new concept. The major focus on the surface modification to augment CHF and boiling heat transfer has been on the microscale modifications [9–11]. These microstructure modifications have some disadvantages, for example, they reduce thermal stress and thermal resistance. To reduce these microstructure disadvantages of the surfaces as well as to impose an effective control over the surface roughness and porosity, the nanoscale modifications have been recommended.

In this study, to create a nanocoating on the surfaces, the EPD has been used. The EPD technique is utilized in the novel processing of painting, coating, and advanced ceramic

materials [12]. Recently, because of its cost-effective quality and simple apparatus as well as its high versatility to be used with different materials, this contrivance has gained ever-increasing attention in industry and academic investigations. In this technique, the charged nanoparticles dispersed in a base fluid are exposed to DC electric field, and then they are attracted and deposited onto one of the electrodes. Particles with negative charge deposited on the positive electrode (anode) are termed as the anodic EPD, and for positive charge particles, there is cathodic deposition.

In this study, the deposition of SiO_2 nanoparticles with anodic EPD is investigated. The deposition was scrutinized on stainless steel in various nanoparticle depositions, voltage ranges, and deposition times. The thickness of the deposition and the composition of the layer are analyzed by a scanning electron microscope (SEM) and electron energy loss spectroscopy (ELS).

2. Experimental Procedure

2.1. Preparation of Nanofluid. SiO_2 nanoparticles with deionized water were used to produce nanofluids. Charlot et al. [13] measured a constant high ξ potential (-30 ± 5 mV) with a PH of 10 for SiO_2 nanofluid. Therefore, to achieve this PH, the alkali medium was obtained using a NaOH aqueous solution. A stable and monodisperse suspension required for reproducible EPD experiments was produced by this procedure. The fluid containing nanoparticles was stirred well before being placed in the ultrasonic processor, which was run at 2 A and a frequency of 50 Hz for 30 min.

2.2. Electrophoretic Deposition Setup. A plates (4 mm in width and 90 mm in length) made of stainless steel were used as boiling surfaces. Two stainless steel plates, acting as electrodes, with 5 mm distance were connected to a 0–50 V DC power supply. Since a negative zeta potential was measured for the SiO_2 particles, the surface that was to be coated was attached to the cathode electrode. The EPD setup that the wires submerged in SiO_2 nanofluid is shown in Figure 1. Before the boiling tests, the coated surfaces were allowed to dry for one day.

2.3. Pool Boiling Setup. A schematic diagram of the pool boiling setup is shown in Figure 2. As shown in this figure, the boiling heat transfer and the CHF were measured for coated and uncoated stainless steel plates at atmospheric pressure. A fluid pool, electric heater, copper leads, condenser, holder, RTD thermometer, DC power supply, and narrow plates were used in the test setup. The test sample temperature was measured using the temperature coefficient of the resistance method. The temperature coefficient of resistance describes the relative change of the resistance per degree of the temperature change. The relation between the resistance and temperature was correlated by

$$\frac{R(T)}{R(T_0)} = 1 + \alpha \Delta T. \tag{1}$$

The stainless steel temperature coefficient of resistance was determined to be $0.0006 \pm 0.00005\,\mathrm{K}^{-1}$ over the 25–160°C temperature range. Because of the high thermal conductivity and low thickness of stainless steel, the Biot number was determined to be less than 0.1, implying that the lump capacitance analysis could be used.

$$q'' = h_{\mathrm{eff}} (T_W - T_{\mathrm{sat}}). \tag{2}$$

The pool temperature was adjusted by the heater. The heat flux of the test sample was increased by step increasing of the power supply voltage. This condition continued until the test sample failed; in other words, the CHF was observed at this point. The test sample heat flux was calculated by

$$q'' = \frac{IV}{A}. \tag{3}$$

The boiling heat flux and test sample temperature were recorded to plot the boiling curve and calculate the heat transfer coefficient in every step of the power loading.

To investigate the uncertainty of the CHF measurement, the Kline and McClintock [14] uncertainty analysis method is used as follows:

$$\frac{w_{q''}}{q''} = \sqrt{\left(\frac{w_I}{I}\right)^2 + \left(\frac{w_v}{V}\right)^2 + \left(\frac{w_A}{A}\right)^2}. \tag{4}$$

The uncertainty for voltage and current was typically 1% and for cross section was 1.1%. The uncertainty in the thermal flux is 1.8%. Measurement uncertainty for wall superheat was 15%.

3. Results and Discussion

3.1. Contact Angle Measurements. The contact angle is usually measured, where a solid surface contacts with a liquid droplet, to determine the wettability of that surface. The relative molecular interaction strength between vapor, liquid, and solid is reflected by the equilibrium contact angle. The Young [15] equation determines the contact angle for the perfectly flat surface:

$$\gamma_{\mathrm{SG}} - \gamma_{\mathrm{SL}} - \gamma_{\mathrm{LG}} \cos\theta_C = 0. \tag{5}$$

The wettability is significantly affected by the surface roughness and contamination, whereby the Young equation is not globally valid for these surfaces. However, for more or less rugged surface, if it is wetted homogenously, the contact angle can be determined by the Wenzel [16] correlation.

$$\cos(\theta_m) = r \cos(\theta_C), \tag{6}$$

where r is the roughness ratio and is determined as the actual surface area divided by the projected area.

In order to study this phenomenon, the contact angle was measured by the Stalder [17] technique. Figure 3 shows a drop of pure water contact angle with the coated and uncoated surfaces. As shown in this figure, increasing the EPD time or increasing the thickness of the coating, the contact angle was decreased; in other words, the wettability of surfaces increased with SiO_2 nanocoating.

3.2. Effect of Sintering. Four plates coated with EPD were sintered in 200, 500, 700, and 800 degrees of centigrade for 5 hours. Sintering, the process of compacting and forming the

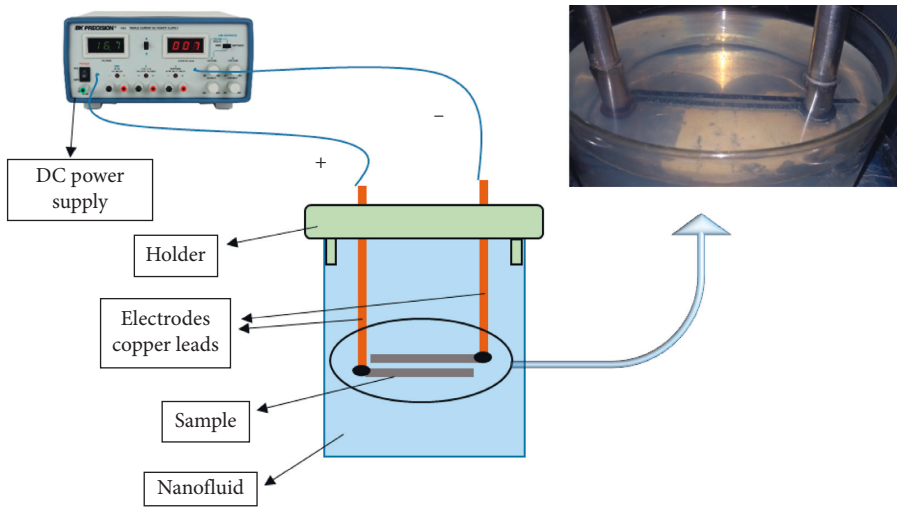

Figure 1: A schematic of EPD setup.

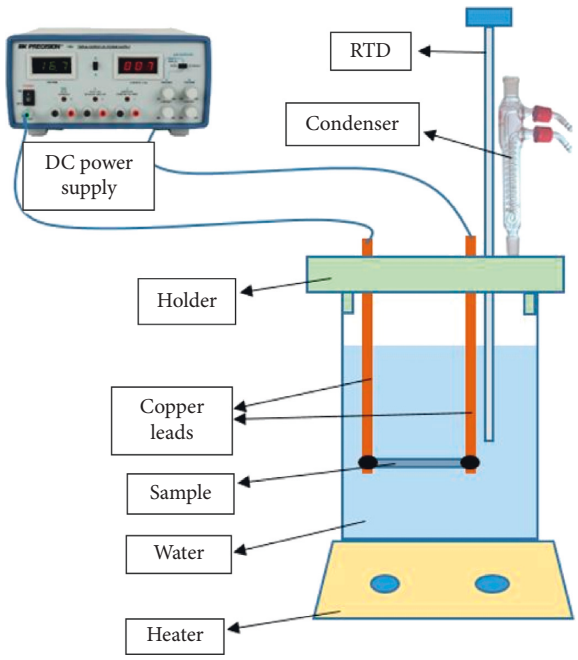

Figure 2: A schematic diagram of the boiling test.

particles by heat or pressure without melting them, is one of the methods of increasing the strength and durability of the nanoparticle coating. As shown in Figure 4, sintering has a significant effect on the contact angle, according to Forrest et al. [18]; the surface is converted to a super-hydrophilic surface by sintering. Table 1 shows the contact angle of various coated plates.

3.3. Coating Thickness. To understand the deposition process, the kinetic deposition of EPD can be used. Initially, when the deposition resistance is not increased, the deposition can be correlated by the linear Hamaker [19] law. Hamaker explained his experimental measurements with linear EPD kinetics and showed that the mass of the deposition linearly depends on the suspension properties and can be written as

$$z = \frac{C\mu_e Et}{\rho}. \tag{7}$$

To determine the thickness of SiO_2 nanocoating, the cross section SEM images were captured. In a microscale view shown in Figure 5, the coating is homogenous and smooth. Figure 6 shows the thickness of the deposition with the two percentage of the nanofluid. As shown in this figure, the coating thickness is strongly affected by the particle percentage in the nanofluid. Figure 7 shows the SEM images of electrophoretic deposition at various deposition times, and it can be noted that the mass of deposition increases with time. A comparison between the thicknesses of silica nanocoating versus time, as made in this study, and Charlot et al. [20] experiment trend line are shown in Figure 8(a). In Figure 8(b), the thickness versus concentration is compared with the Hamaker model, equation (7).

In Figure 8(a), the coating experimental results of this study are compared with the experimental data of Charlot et al. [20] at 0.5% concentration. This figure shows that results compare well. However, Figure 8(b) shows that increasing the nanofluid concentration, the Hamaker model predicts the measured coating thickness. This finding indicates that the control of the coating thickness is easier at lower concentrations, and therefore, the EPD and subsequent experimental tests were conducted at lower concentrations.

3.4. Pool Boiling Results. As shown in Table 1, the contact angle of the coated plates was decreased; therefore, the surfaces become hydrophilic and super-hydrophilic. The boiling curve obtained for the bare and SiO_2 coated plates is shown in Figure 9. The significant increment at the superheat temperature of the wall for the hydrophilic plates is conspicuous. The effect of sintering on the boiling of the coated plates is demonstrated in Figure 10. As shown in the figure, the superheat temperature under the nucleate boiling

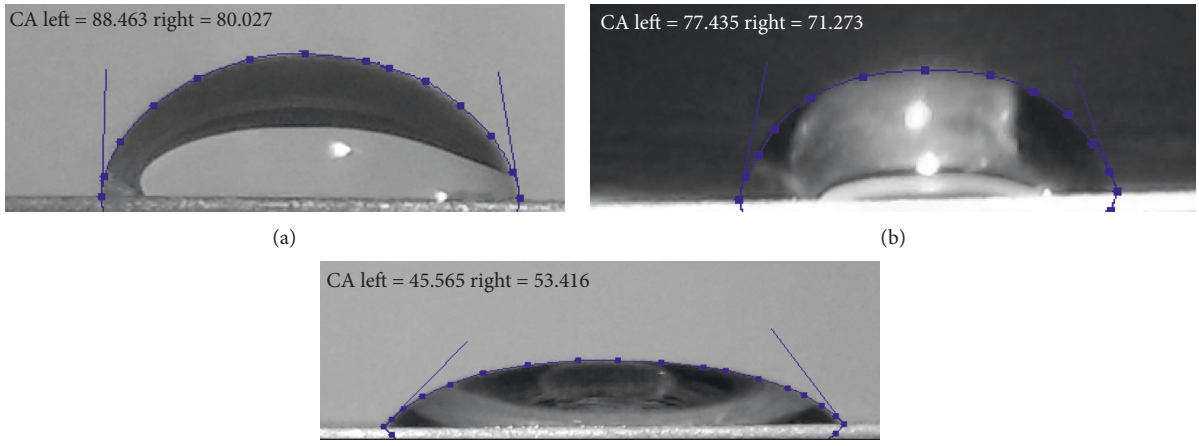

Figure 3: Static contact angles of pure water on stainless steel plates for (a) clean surface and (b) 20 minutes and (c) 60 minutes EPD coating.

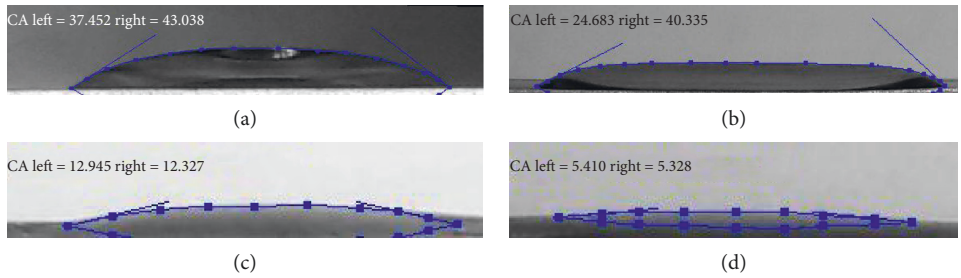

Figure 4: Static contact angles of pure water on stainless steel plates for (a) 200°C, (b) 500°C, (c) 700°C, and (d) 800°C.

Table 1: Contact angle and thickness of various coated surfaces.

Case	Contact angle (°C)
Bare plate	88.4
20 minute with 0.5% nanofluid	77.4
60 minute with 0.5% nanofluid	45.5
Sintered at 200°C	37.4
Sintered at 500°C	24.6
Sintered at 700°C	12.9
Sintered at 800°C	5.4

regime is decreased at low sintering temperatures (200 and 500°C) and is significantly increased at high sintering temperatures (700 and 800°C). In the course of this study, the effects of the modified surfaces created by the EPD technique on the nucleate boiling heat transfer and the CHF have been investigated.

3.4.1. Heat Transfer Coefficient. As depicted in Figures 9 and 10, the boiling curves of the coated plates tend to shift to higher wall superheat than the clean surface in the nucleate boiling regime. This implies that decreasing the surface contact angle or increasing wettability obtained by coating and then sintering (Table 1), as Wang and Dhir [21] predicted, the nucleate boiling heat transfer occurs at higher surface temperatures, whereas the boiling heat transfer coefficient is decreased.

Figure 11 implies that the nucleate heat transfer coefficient is decreased with various coated surfaces which have lower contact angle than bare surface. The heat transfer coefficient versus heat flux for bare and sintered surfaces (first 40 min EPD coating and then sintered at 200, 500, 700, and 800°C) is shown in Figure 12. However, it can be seen in this figure that for two sintered plates (200 and 500°C), the heat transfer is enhanced compared to coated and unsintered surfaces.

Particle adhesion to each other and to heating surface at low sintering temperatures increases without affecting or decreasing the surface porosity. This phenomenon increases the heat transfer coefficient compared to the unsintered surfaces. However, increasing the sintering temperature, the particles surface melting rate increases and the porous layer and the capillary suction both decrease. On the other hand, the reduction of the nucleation site density due to the reduction of the porosity and capillary suctions lead to the reduction of the heat transfer coefficient.

To explain these processes, the widely used Mikic and Rohsenow [22] nucleate boiling heat transfer correlation can be used:

$$q = \frac{1}{2}\left(\pi k_l \rho c_p\right)^{1/2} f^{1/2} D_d^2 n_a \Delta T_s, \tag{8}$$

$$\Delta T_s = \frac{q}{1/2\left(\pi k_l \rho c_p\right)^{1/2} f^{1/2} D_d^2 n_a}. \tag{9}$$

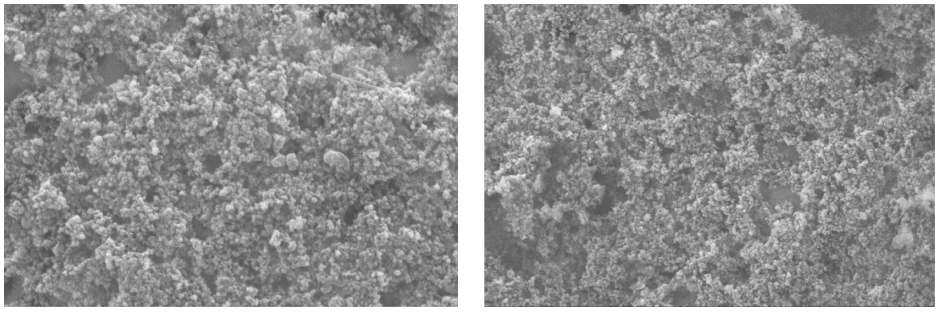

(a) (b)

Figure 5: SEM images of stainless steel coating for (a) 200°C and (b) 500°C.

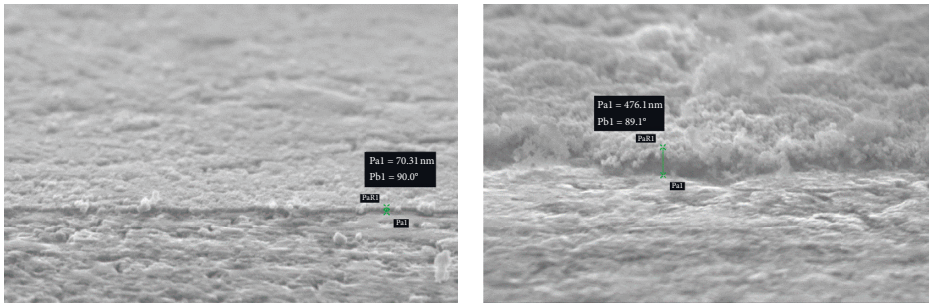

(a) (b)

Figure 6: SEM images of electrophoretic deposition with (a) 0.5% and (b) 2.0% nanofluid percentage.

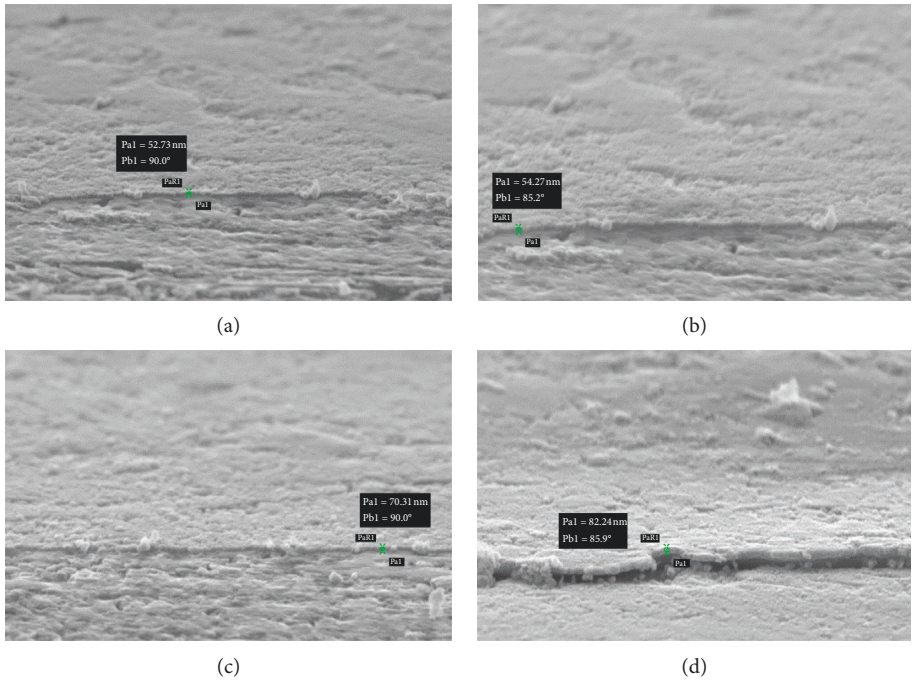

(a) (b)

(c) (d)

Figure 7: SEM images of electrophoretic deposition with (a) 20-, (b) 30-, (c) 40-, and (d) 60-minute deposition time.

As shown in equation (9), the surface superheat temperature or the heat transfer coefficient depends on the nucleation site density, bubble departure diameter, and bubble departure frequency. Phan et al. [23] observed that the nucleation site density remains almost constant with changing of the contact angle at averaged time period.

The departure bubble diameter widely predicted by the Fritz [24] correlation is

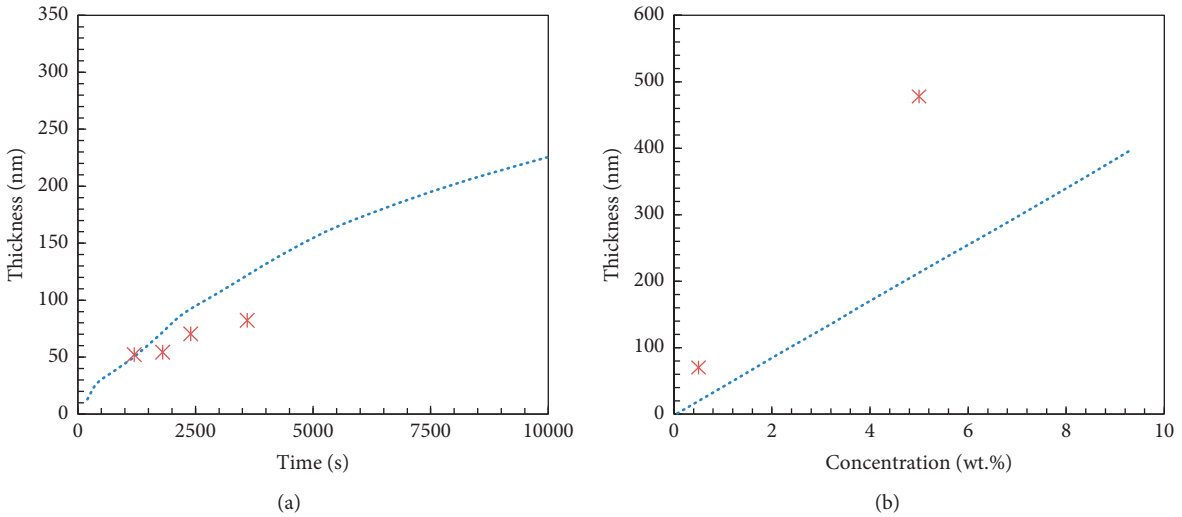

Figure 8: Thickness silica nanocoating versus (a) deposition time (dash line is the trend line in Charlot et al. experiment [20]) and (b) concentration (dash line is the Hamaker model [19]).

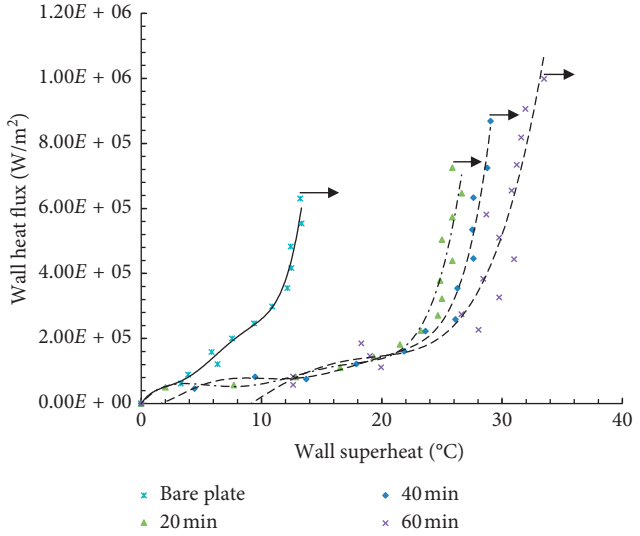

Figure 9: Pool boiling curves for bare and coated plates.

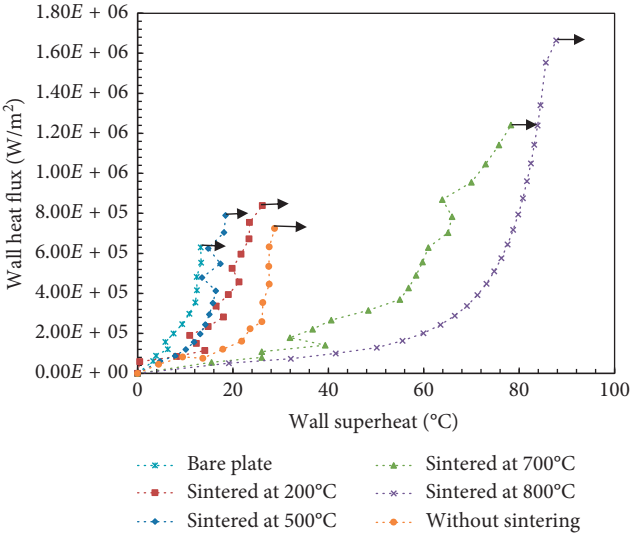

Figure 10: Pool boiling curves for bare and sintered plates.

$$d_{\mathrm{Bd}} = 0.0208\theta\sqrt{\frac{\sigma}{g\Delta\rho}}. \tag{10}$$

Equation (10) relates only the fluid properties and the gravity effects and shows the maximum bubble volume as a function of capillary length and contact angle. The bubble departure is determined by surface tension and buoyancy forces. Hypothetically, the departure occurs when buoyancy overcomes the surface tension, inertia, and drag forces that prevent the detachment of the bubbles.

Phan et al. [23] obtained a correlation that incorporates the Fritz model assumptions with the influence of the energy factor as the contribution of the wetting effects:

$$f(\theta) = \frac{2 + 3\cos\theta - \cos^3\theta}{4}, \tag{11}$$

$$D_d = 0.626977 f(\theta)\left(\frac{\sigma}{g(\rho_l - \rho_v)}\right)^{1/2}, \tag{12}$$

where $f(\theta)$ is a volume ratio between a truncated sphere and a complete sphere with equal diameter. Equation (12) shows that the bubble diameter increases with increasing surface wettability. The required energy to activate nucleate sites as well as the growth time (t_g) and the waiting time (t_w) is increased for the bigger bubbles. The bubble departure frequency can be written by

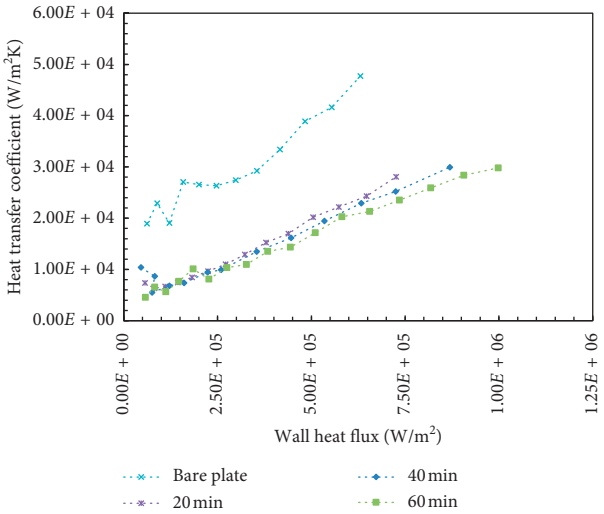

Figure 11: Heat transfer coefficient versus heat flux for bare and coated plates.

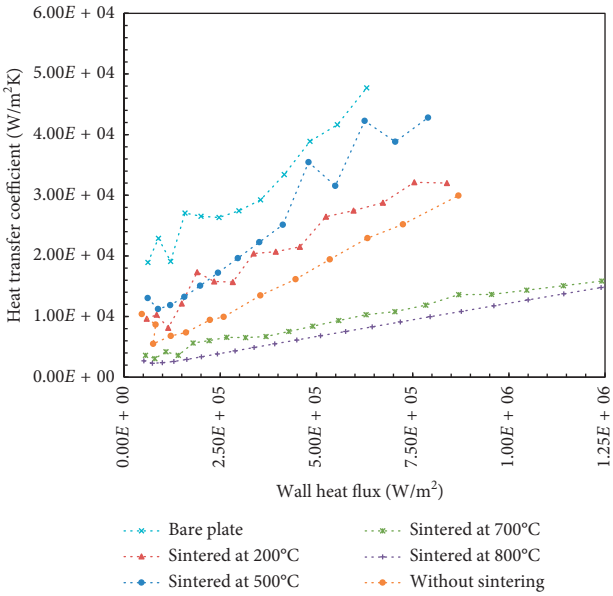

Figure 12: Heat transfer coefficient versus heat flux for bare and sintered plates (first forty minutes EPD coating and then sintered at 200, 500, 700, and 800°C).

$$f = \frac{1}{t_g + t_w}. \tag{13}$$

In other words, at higher surface wettability, the bubble departure frequency decreases, but the bubble diameter increases. Figure 13 shows the bubble departure frequency and bubble diameter versus the contact angle from Phan et al. [23, 25] studies.

As shown in Figure 13, the bubble departure frequency, between 70 and 90 degrees and lower than 10 degrees, has the highest slip reduction, but the bubble diameter is reduced between 50 and 90, and for lower than 50, it becomes almost a constant value. The wall superheat increment at higher wettability can also be explained using equation (9).

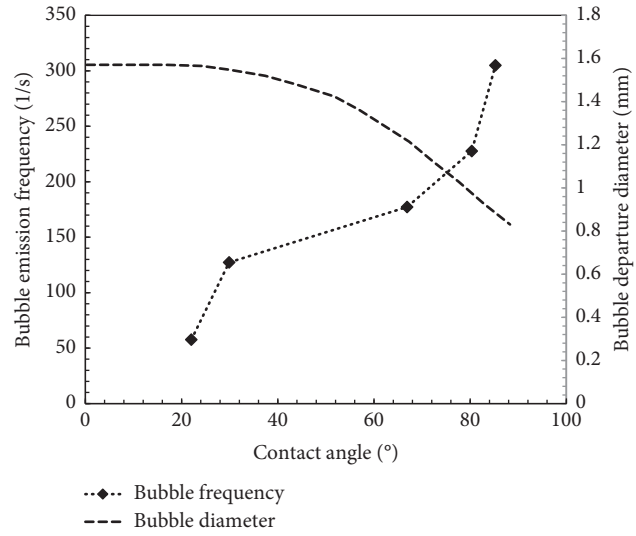

Figure 13: Frequency of bubble departure and bubble diameter versus the contact angle [23, 25].

In this study, for better understanding, the heat transfer coefficient versus contact angle for various heat fluxes is shown in Figure 14. It can be deduced that the effect of bubble departure frequency on the heat transfer coefficient at the contact angle range of 90°–70° and lower than 30° is dominant, as reported by Phan et al. [23, 25].

For hydrophilic surfaces, the effect of liquid microlayer underneath the bubble is an important parameter that the bigger area of liquid microlayer and lower thickness of microlayer improve the heat transfer coefficient. Therefore, the competition between the area and the thickness of the liquid microlayer with the bubble departure frequency affect the outcome of the heat transfer coefficient for hydrophilic and super-hydrophilic surfaces.

3.4.2. CHF. The CHF represents the boiling crisis and the peak heat flux which a heated section possesses without the loss of macroscopic physical contact between the heated surface and the liquid. For the industrial systems, the CHF determines the upper limit for the safe operation. Zuber [26] modeled the CHF of pool boiling based on the hydrodynamic instability theory. For many years, the CHF or departure from the nucleate boiling (DNB) was modeled by the Zuber correlation:

$$q''_{\mathrm{CHF}} = K\rho_g h_{fg}\left[\frac{g\sigma\left(\rho_f - \rho_g\right)}{\rho_g^2}\right]^{1/4}, \tag{14}$$

where K depends on the system geometry.

According to the hydrodynamic theory, the CHF is a Tailor-driven process and the vapor jets have the highest Helmholz instability velocity that arises at the nodes of the Taylor waves. The hydrodynamic theory only depends on the fluids properties and does not consider the surface parameter such as wettability and surface modifications. Figure 9 illustrates that the CHF increases by the nanoparticle deposition on the heated surface; it also shows the limitation of the Zuber model.

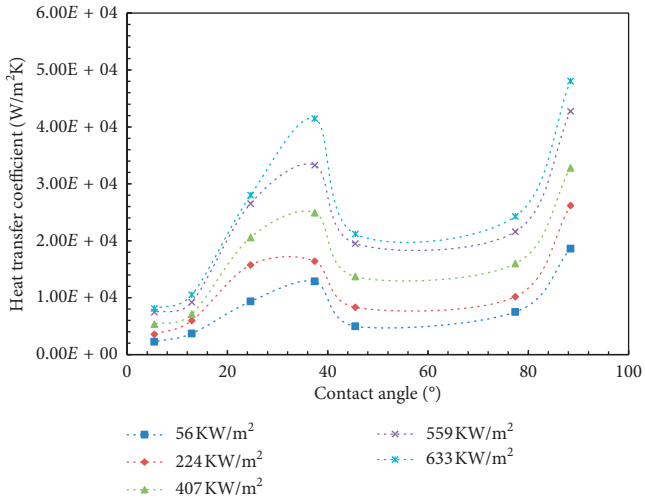

Figure 14: Heat transfer coefficient versus the contact angle.

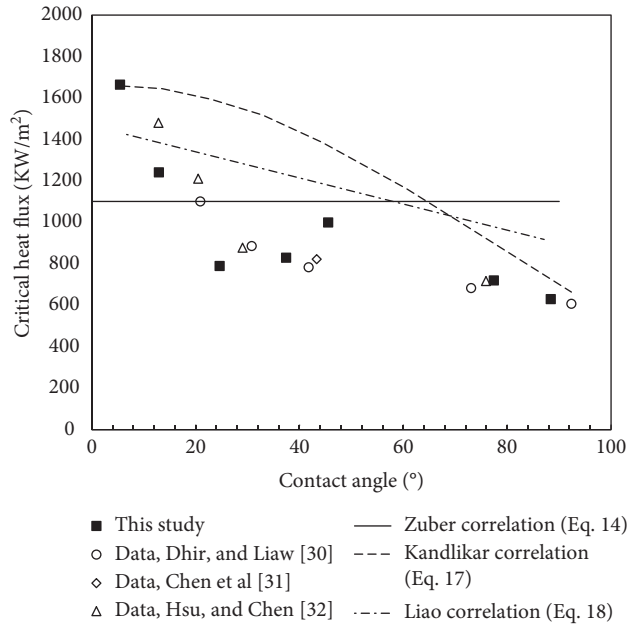

Figure 15: Critical heat flux versus contact angle.

The hot/dry spot theory proposed by Theofanous and Dinh [27] is one of the theories that investigate the surface parameters. According to this theory, CHF develops when rewetting is unable to occur at a growing hot spot. The CHF proposed by this theory is

$$q''_{\mathrm{CHF}} = \kappa^{-(1/2)} \rho_g h_{fg} \left[\frac{g\sigma(\rho_f - \rho_g)}{\rho_g^2}\right]^{1/4}, \quad (15)$$

where κ is a constant which depends on the surface parameter and is explicitly obtained by Jun et al. [5].

$$\kappa = \left(1 - \frac{\sin\theta}{2} - \frac{(\pi/2) - \theta}{2\cos\theta}\right)^{-(1/2)}. \quad (16)$$

This correlation is only valid for hydrophilic surfaces.

Another correlation that depends on the surface parameter is the Kandlikar [28] model which can be used for all contact angles.

$$q''_{\mathrm{CHF}} = \rho_g^{1/2} h_{fg} \left(\frac{1+\cos\beta}{16}\right) \times \left[\frac{2}{\pi} + \frac{\pi}{4}(1+\cos\beta)\cos\phi\right]^{1/2} \cdot \left[\sigma g(\rho_f - \rho_g)\right]^{1/4}, \quad (17)$$

where β is the receding contact angle.

Liao et al. [29] represented the Zuber CHF correlation with the effect of orientation and contact angle:

$$q''_{\mathrm{CHF}} = \left[1 + \frac{55-\theta}{100}(0.56)\right] \rho_g h_{fg} \left[\frac{g\sigma(\rho_f - \rho_g)}{\rho_g^2}\right]^{1/4}. \quad (18)$$

A comparison between the CHFs obtained in this study, the three CHF correlations (15), (17), and (18), and the experimental data [30–32] as a function of the contact angle is shown in Figure 15.

The Zuber model predicts the constant CHF value, but the Kandlikar and the Liao CHF correlations are not constant, and the CHF decreases with the increase in contact angle. These reductions are linear in the Liao correlation and are nonlinear in the Kandlikar correlation. The Kandlikar correlation overpredicts the CHF experimental data. However, the CHF results of this study are closer to those of Hsu and Chen [32].

4. Conclusion

In this investigation, the EPD on thin plates was used to study the critical heat flux behavior in a pool boiling experiment. Because of the negatively charged particles, the particles deposited on the anodic electrode. The main findings of the present investigation can be summarized as follows:

(i) The EPD technique, due to the setup simplicity, shape independency, uniformity of particle coating, and controllability of thickness, can be an appropriate option for modification of the surface and coating on the nuclear fuel cladding.

(ii) The heat transfer coefficient of the nanocoated surfaces decreased from 27 to 11 kW/m^{2}K at 298 kW/m^2 wall heat flux by nearly 100%.

(iii) Increasing the deposition time and increasing the coating thickness (up to 90 nm for 0.5% nanofluid) increased the CHF.

(iv) The results obtained in this study show that the Kandlikar correlation overpredicts (on average about 30%) the CHF for nanocoated surfaces.

(v) The CHF of the nanocoated surfaces increased from 630 to 1000 kW/m^2 by 58% and increased from 1000 to 1664 kW/m^2 by 60% for sintered surfaces.

Nomenclature

C: Concentration (g/cm^3)
d: Diameter
E: Electric field (V/cm)
f: Frequency
g: Gravity acceleration (m/s^2)
h: Enthalpy (J/kg)
N: Nucleation site density
I: Ampere (A)
q'': Heat flux (W/m^2)
R: Resistance (Ω)
T: Temperature (°C)
t: Time (s)
V: Voltage (volt)
Z: Thickness (cm).

Greek Letters
ρ: Density (g/cm^3)
μ: Electrophoretic mobility (cm^2/V·s)
γ: Surface energy
θ: Contact angle (radian)
σ: Surface tension.

Subscripts
B: Bubble
CHF: Critical heat flux
eff: Effective
W: Wall
Sat: Saturate
S: Solid
L: Liquid
G: Gas or vapor.

Data Availability

The data used to support the findings of this study are available from the corresponding author upon request

Additional Points

Highlights. (i) An anodic electrophoretic deposition (EPD) was used as nanoparticle coating. (ii) The hydrophilic and super-hydrophilic surfaces were established by SiO_2 coating. (iii) Higher strength and CHF were obtained by sintering of the coated surfaces. (iv) The BHT and CHF behaviors of hydrophilic and super-hydrophilic surfaces have been investigated. (v) The EPD technique could be an appropriate option for coating of nuclear fuel claddings.

Conflicts of Interest

The authors declare that they have no conflicts of interest.

References

[1] S. Choi, "Enhancing thermal conductivity of fluids with nanoparticles," in *Developments and Applications of Non-newtonian Flows, ASME, FED-231/MD-66*, D. A. Siginer and H. P. Wang, Eds., pp. 99–105, 1995.

[2] B. Truong, L. W. Hu, and J. Buongiorno, "Surface modifications using nanofluids for nucleate boiling heat transfer and CHF enhancements," in *Proceedings of the Sixth International ASME Conference on Nanochannels, Microchannels and Minichannels, ICNMM2008*, Darmstadt, Germany, June 2008.

[3] K. Hadad, A. Rahimian, and M. R. Nematollahi, "Numerical study of single and two-phase models of water/Al_2O_3 nanofluid turbulent forced convection flow in VVER-1000 nuclear reactor," *Annals of Nuclear Energy*, vol. 60, pp. 287–294, 2013.

[4] B. A. K. Naik and A. V. Vinod, "Heat transfer enhancement using non-Newtonian nanofluids in a shell and helical coil heat exchanger," *Experimental Thermal and Fluid Science*, vol. 90, pp. 132–142, 2018.

[5] S. Jun, J. Kim, S. M. You, and H. Y. Kim, "Effect of subcooling on pool boiling of water from sintered copper microporous coating at different orientations," *Science and Technology of Nuclear Installations*, vol. 2018, Article ID 8623985, 9 pages, 2018.

[6] W. Zhao, X. Zhang, C. Tian, and Z. Gao, "Analysis of wetting characteristics on microstructured hydrophobic surfaces for the passive containment cooling system," *Science and Technology of Nuclear Installations*, vol. 2015, Article ID 652731, 6 pages, 2015.

[7] R. N. Hegde, S. S. Rao, and R. P. Reddy, "Studies on nanoparticle coating due to boiling induced precipitation and its effect on heat transfer enhancement on a vertical cylindrical surface," *Experimental Thermal and Fluid Science*, vol. 38, pp. 229–236, 2012.

[8] H. S. Ahn, S. H. Kang, and M. H. Kim, "Visualized effect of alumina nanoparticles surface deposition on water flow boiling heat transfer," *Experimental Thermal and Fluid Science*, vol. 37, pp. 154–163, 2012.

[9] P. J. Berenson, "Experiments on pool-boiling heat transfer," *International Journal of Heat and Mass Transfer*, vol. 5, no. 10, pp. 985–999, 1962.

[10] G.-S. Hwang and M. Kaviany, "Surface wettability change during pool boiling of nanofluids and its effect on critical heat flux," *International Journal of Heat and Mass Transfer*, vol. 49, no. 5-6, pp. 844–849, 2006.

[11] M. Shojaeian and A. Koşar, "Pool boiling and flow boiling on micro- and nanostructured surfaces," *Experimental Thermal and Fluid Science*, vol. 63, pp. 45–73, 2015.

[12] G. E. F. Brewer, "Electrophoretic painting," *Journal of Applied Electrochemistry*, vol. 13, no. 3, pp. 269–275, 1983.

[13] A. Charlot, X. Deschanels, and G. Toquer, "Submicron coating of SiO_2 nanoparticles from electrophoretic deposition," *Thin Solid Films*, vol. 553, pp. 148–152, 2014.

[14] S. J. Kline, "Describing uncertainty in single sample experiments," *Mechanical Engineering*, vol. 75, pp. 3–8, 1953.

[15] T. Young, "An essay on the cohesion of fluids," *Philosophical Transactions of the Royal Society of London*, vol. 95, pp. 65–87, 1805.

[16] R. N. Wenzel, "Resistance of solid surfaces to wetting by water," *Industrial & Engineering Chemistry*, vol. 28, no. 8, pp. 988–994, 1936.

[17] A. F. Stalder, G. Kulik, D. Sage, L. Barbieri, and P. Hoffmann, "A snake-based approach to accurate determination of both contact points and contact angles," *Colloids And Surfaces A: Physicochemical And Engineering Aspects*, vol. 286, no. 1–3, pp. 92–103, 2006.

[18] E. Forrest, E. Williamson, J. Buongiorno, L.-W. Hu, M. Rubner, and R. Cohen, "Augmentation of nucleate boiling heat transfer and critical heat flux using nanoparticle thin-film

coatings," *International Journal of Heat and Mass Transfer*, vol. 53, no. 1–3, pp. 58–67, 2010.

[19] H. C. Hamaker, "Formation of a deposit by electrophoresis," *Transactions of the Faraday Society*, vol. 35, pp. 279–283, 1940.

[20] A. Charlot, X. Deschanels, and G. Toquer, "Submicron coating of SiO_2 nanoparticles from electrophoretic deposition," *Thin Solid Films*, vol. 553, pp. 148–152, 2014.

[21] C. H. Wang and V. K. Dhir, "Effect of surface wettability on active nucleation site density during pool boiling of water on a vertical surface," *Journal of Heat Transfer*, vol. 115, no. 3, pp. 659–669, 1993.

[22] B. B. Mikic and W. M. Rohsenow, "A new correlation of pool-boiling data including the effect of heating surface characteristics," *Journal of Heat Transfer*, vol. 91, no. 2, pp. 245–250, 1969.

[23] H. T. Phan, N. Caney, P. Marty, S. Colasson, and J. Gavillet, "Surface wettability control by nanocoating: the effects on pool boiling heat transfer and nucleation mechanism," *International Journal of Heat and Mass Transfer*, vol. 52, no. 23-24, pp. 5459–5471, 2009.

[24] W. Fritz, "Maximum volume of vapour bubbles," *Physikalische Zeitschrift*, vol. 36, pp. 379–384, 1935.

[25] H. T. Phan, N. Caney, P. Marty, S. Colasson, and J. Gavillet, "How does surface wettability influence nucleate boiling?," *Comptes Rendus Mécanique*, vol. 337, no. 5, pp. 251–259, 2009.

[26] N. Zuber, *Hydrodynamic Aspects of Boiling Heat Transfer, AECU-4439*, Atomic Energy Commission, Los Angeles, CA, USA, 1959.

[27] T. G. Theofanous and T. N. Dinh, "High heat flux boiling and burnout as microphysical phenomena: mounting evidence and opportunities," *Multiphase Science and Technology*, vol. 18, no. 3, pp. 251–276, 2006.

[28] S. G. Kandlikar, "A theoretical model to predict pool boiling CHF incorporating effects of contact angle and orientation," *Journal of Heat Transfer*, vol. 123, no. 6, pp. 1071–1079, 2001.

[29] L. Liao, R. Bao, and Z. Liu, "Compositive effects of orientation and contact angle on critical heat flux in pool boiling of water," *Heat and Mass Transfer*, vol. 44, no. 12, pp. 1447–1453, 2008.

[30] V. K. Dhir and S. P. Liaw, "Framework for a unified model for nucleate and transition pool boiling," *Journal of Heat Transfer*, vol. 111, no. 3, pp. 739–746, 1989.

[31] R. Chen, M.-C. Lu, V. Srinivasan, Z. Wang, H. H. Cho, and A. Majumdar, "Nanowires for enhanced boiling heat transfer," *Nano Letters*, vol. 9, no. 2, pp. 548–553, 2009.

[32] C. C. Hsu and P. H. Chen, "Surface wettability effects on critical heat flux of boiling heat transfer using nanoparticle coatings," *International Journal of Heat and Mass Transfer*, vol. 55, no. 13-14, pp. 3713–3719, 2012.